PCCP

Accepted Manuscript

ROYAL SOCIETY OF CHEMISTRY

www.rsc.org/pccp

Physical Chemistry Chemical Physics

Cite this: DOI: 10.1039/c0xx00000x

www.rsc.org/pccp

PAPER

The relationship of boron dipyrromethene (BODIPY) structure to the effectiveness of homogeneous and heterogeneous solar hydrogen-generating systems as well as DSSCs†

Geng-Geng Luo,*[a] Hui Lu,[a] Xiao-Long Zhang,[a] Jing-Cao Dai,[a] Ji-Huai Wu[a] and Jia-Jia Wu[a]

Received (in XXX, XXX) Xth XXXXXXXXX 2015, Accepted Xth XXXXXXXXX 2015
First published on the web Xth XXXXXXXXX 2015
DOI: 10.1039/b000000x

A series of boron dipyrromethene (BODIPY) dyes (**B1**-**B5**) having H atoms at 2,6-positions or heavy-atom I at 2-/2,6-positions, and *ortho*- or *para*-COOH substituted phenyl moiety at the 8-position on the BODIPY core were synthesized and characterized. These organic dyes were applied to investigating the relationship of BODIPY structure to the effectiveness of homogeneous and heterogeneous visible-light-driven hydrogen production as well as dye-sensitized solar cells (DSSCs). For the homogeneous photocatalytic hydrogen production systems with a cobaloxime catalyst, the efficiency of hydrogen production could be tuned by substituting with heavy atoms and varying carboxyl group orientations of BODIPYs. As a result, **B5** containing two I atoms and an *ortho*-COOH anchoring group was the most active one (TONs = 197). The activity of hydrogen generation followed the order **B5** > **B3** > **B2** > **B1** = **B4** = 0. An interesting "*ortho*-position effect" was observed in the present homogeneous systems, i.e., substition groups were located at the *ortho*-position, higher hydrogen production activities were obtained. For the heterogeneous hydrogen production systems with a platinized TiO_2 catalyst, the effectiveness of hydrogen evolution was highly influenced by the intersystem crossing efficiency, molar absorptivity and positions of anchoring group of dyes. Thus, **B3** having two core iodine atoms and a *para*-COOH group with TONs of 70 excelled other BODIPYs and the TONs of hydrogen generation showed the trend of **B3** > **B5** > **B2** > **B1** = **B4** = 0. The results demonstrate that the present photocatalytic H_2 production proceeds with higher efficiency and stability in the homogeneity than in the heterogeneity. In the case of DSSCs, the overall cell performance of BODIPY chromophores were highly dependent on both absence or presence of iodine atoms on the BODIPY core and –COOH anchoring positions. The **B1**-TiO_2 system showed the best cell performance, because the most effective surface binding mode is allowed with this structure. This is also contrasted with the case of dye-sensitized solar H_2 generation, in which **B3** was the most efficient chromophore. The differences between dye-sensitized hydrogen-generating systems and DSSCs may be due to rates of electron transfer and the dye aggregation tendency.

1. Introduction

With the rapid and continuing development of industrial society, the global energy crisis has become a major concern to the public in recent yeats. Solar energy is the most abundant sustainable energy resource. Harnessing solar energy is a potential choice to solve today's energy issues, with much attention and effort focused on solar-driven photocatalytic hydrogen production and dye-sensitized solar cells (DSSCs). Hydrogen generation from water under solar irradiation includes homogeneous and heterogeneous catalytic systems, and is regarded as one of the Holy Grails of 21st century chemistry, being one route to a fuel that is not derived from fossil fuels and a potential source of clean and renewable energy to satisfy the rising global energy demand.[1] DSSCs, often known as Grätzel cells, have garnered significant attention as promising low-cost alternatives for the photovoltaic conversion of solar energy.[2] A crucial issue in solar hydrogen production and DSSCs design is the choice of photosensitizers used to capture the solar energy. Although many novel structures have been developed and tested as light absorbers in photocatalytic hydrogen generation and DSSCs, complexes of ruthenium and other noble metals (Ir, Pt) as light absorbers remain dominant in the most successful systems.[3,4] However, despite the desirable redox properties of noble-metal complexes excited states, their relatively expensive, hard to purify and low molar absorptivities (< 20000 M^{-1} cm^{-1}) represent a drawback in their use for the utilization of solar energy.[5]

As an alternative to noble-metal complexes, organic dyes are becoming more and more attractive due to many advantages, such as diversity of molecule structures, high extinction coefficients leading to great light harvesting abilities, simple

[a]*College of Materials Science and Engineering, Huaqiao University, Xiamen 361021, P. R. China*;
Fax: 86-592-6162225 E-mail: ggluo@hqu.edu.cn;
†Electronic Supplementary Information (ESI) available. Additional calculations and experimental measurements, table S1-S4, scheme S1-S3 and Fig. S1-S11. CCDC reference numbers 1045034-1045036. For ESI and crystallographic data in CIF or other electronic format see DOI:10.1039/b000000x.

synthesis as well as low cost and environmental issues.[6] However, compared with transition metal complexes, organic dyes have been examined as optical absorbers in the conversion of solar energy on a limited basis.[7] Thus, the search for new, highly efficient based-organic dyes remains an active aspect of solar hydrogen generation and DSSCs development. Among organic dyes, borondifluorodipyrromethene (BODIPY), one kind of brilliant small molecule dye which is structurally based on the half-porphyrin motif but chelated by a difluoroboron moiety to maintain overall structural rigidity, shows distinctly charming photophysical properties that include high extinction coefficients (> 70000 M^{-1} cm^{-1}), weak nonradiative decay of the excited state, and resistance to photobleaching.[8] In addition, ease of functionalization of BODIPY makes it possible to fine-tune the energy levels of the S_1 and T_1 excited state by attaching heavy atoms directly onto the chromophore core to enhance spin orbit coupling.[9] Recently, many researchers have reported BODIPY chormophores in the context of chemsensors, light-emitting materials for electroluminescent devices, photodynamic therapeutics, triplet-triplet annihilation upconversion, photovoltaics, and so forth.[10] However, the study of these chromophores for solar hydrogen-generating systems is scarce.

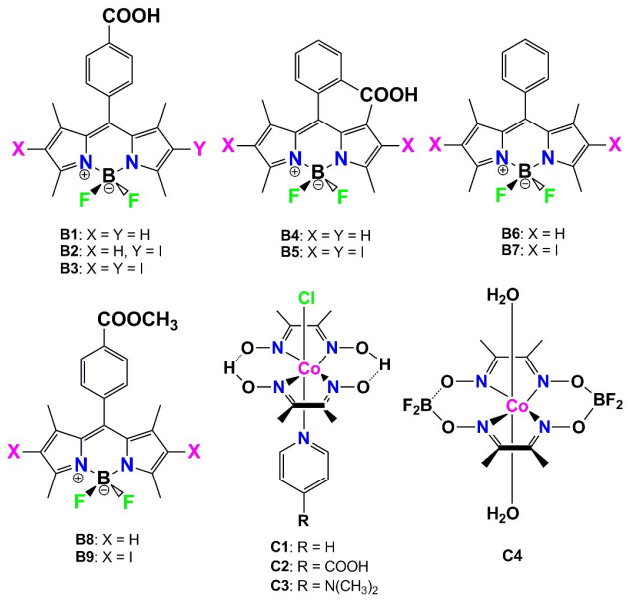

Scheme 1 Structures of BODIPY dyes **Bn** (n = 1-9) and cobaloximes **Cn** (n = 1-4) used in this study.

On the other hand, to date, both solar hydrogen production and DSSCs have been explored separately for solar energy conversion, yet little work has been done on comparing the differences in conditions between homogeneous and heterogeneous solar hydrogen-generating systems as well as DSSCs, and investigating how these differences affect component activity in the systems. Besides, for homogeneous and heterogeneous sunlight-driven hydrogen evolution, we wonder which system would display superior performance of photogeneration H_2 over the counterpart. To this end, in the present study, we prepared a series of BODIPY dyes (**B1**-**B5**) with hydrogen or iodine atoms at 2-position or 2,6-positions, and *ortho*- or *para*-COOH substituted phenyl moiety at the 8-position on the BODIPY core. The detailed structures of dyes are shown in Scheme 1. These based-organic dyes were used for the first time as photosensitizers (PSs) to investigate their influence on the performance of homogeneous and heterogeneous visible-light-driven hydrogen production as well as DSSCs. Detailed investigation on the relationship between the dye structure and effectiveness of solar-driven hydrogen generation and DSSCs is described here.

2. Experimental section

2.1. Materials and methods

All chemical reagents were purchased from commercial suppliers and used without further purification, unless otherwise indicated. Solvents were dried by standard literature methods[11] before being distilled and stored under nitrogen over 3Å molecular sieves prior to use. All air- and moisture-sensitive reactions were carried out under nitrogen atmosphere in oven-dried or flame-dried glassware. TLC was performed on 0.25 mm silica gel 60 F254 TLC plates with a fluorescent indicator at 254 nm excitation. Compounds were visualized under UV light of 254 nm. Column chromatography was performed with silica gel (200-300 mesh). Nanoparticulate TiO_2 was purchased from Degussa. The P25 form is specified to have a nominal particle size of 21 nm, specific surface area of 50 ± 15 m^2 g^{-1}, and a composition of about 70% anatase and 30% rutile.

^1H and ^{13}C NMR spectra were recorded on a Bruker AVANCE III 500 MHz spectrometer in $CDCl_3$ or DMSO-d^6 with shifts referenced to $SiMe_4$ (TMS, 0.00 ppm). Chemical shift multiplicities are reported as s = singlet, d = doublet, and br = broad singlet. Coupling constants (*J*) values are given in Hz. C, H and N microanalyses were carried out with a CE instruments EA 1110 analyzer. Cyclic voltammetry experiments were conducted on a CHI 650E electrochemical analyzer using a three-electrode single-cell compartment at room temperature. All samples were degassed with nitrogen before sampling and blanketed with nitrogen during the run. The working electrode was 2 mm Pt with a Pt wire as auxiliary electrode and a 0.01M $Ag/AgNO_3$ solution reference electrode. The scan rate was 100 mV s^{-1}. The experiments were performed in acetonitrile with 0.1 M tetrabutylammonium hexafluorophosphate (TBAP) used as the supporting electrolyte. Ferrocene was added to each sample solution at the end of the experiments, and the ferrocenium/ferrocene (F_c/F_c^+) redox couple was used as an internal potential reference. Diffuse reflectance UV-vis measurements were taken on a spectrophotometer (Shimadzu, Model UV-2550) with $BaSO_4$ as the reference.

2.2. Spectroscopic measurements and determination of fluorescent life and relative quantum yields

The solvents employed for the spectroscopic measurements were of UV spectroscopic grade (Aldrich). Absorption spectra were recorded using a Shimadzu UV-2100 spectrophotometer (200-800 nm). Steady-state luminescence spectra were measured on a Hitachi F-7000 spectrophotometer with a xenon

arc lamp as light source and corrected for instrument response. Fluorescence decay curves of the samples were measured with the time-correlated single-photon-counting (TCSPC) method on FLSP920 Lifespec-ps (Edinburgh) and the data were analyzed by Edinburgh software. The goodness of the fit of the decays as judged by reduced chi-squared (χ^2_R) and autocorrelation function $C(j)$ of the residuals, was always acceptable yielding values of $\chi^2_R < 1.1$. The fluorescence decay time (τ) was obtained from the slope. Samples for absorption and emission measurements were contained in 1 cm × 1 cm quartz cuvettes. Measurements were made using optically dilute solutions after deoxygenation by purging with dried N_2.

Relative quantum efficiencies of fluorescence of BODIPY derivatives were obtained by comparing the area under the corrected emission spectrum of the test sample with 8-phenyl-4,4-difluoro-1,3,5,7-tetramethyl 4-bora-3a,4a-diaza-*s*-indacene (0.72 in tetrahydrofuran)[12] and Rhodamine B (0.49 in ethanol)[13] as standards, respectively. Dilute solutions ($0.01 < A < 0.05$) were used to minimize the reabsorption effects. The following equation was used to calculate quantum yield:[14]

$$\Phi_{fl}^{sample} = \Phi_{fl}^{standard} \times (I^{sample}/I^{standard}) \times (A^{standard}/A^{sample}) \times (n^{sample}/n^{standard})^2$$

Where Φ_{fl}^{sample} and $\Phi_{fl}^{standard}$ are the emission quantum yields of the sample and the reference, respectively, $A^{standard}$ and A^{sample} are the measured absorbances of the reference and sample at the excitation wavelength, respectively, $I^{standard}$ and I^{sample} are the area under the emission spectra of the reference and sample, respectively, and $n^{standard}$ and n^{sample} are the refractive indices of the solvents of the reference and sample, respectively. The Φ_{fl}^{sample} values reported in this work are the averages of multiple (generally three), fully independent measurements.

2.3. Synthetic procedures

4-(4,4-difluoro-1,3,5,7-tetramethyl-4-bora-3a,4a-diaza-s-indacene-8-yl)-benzoic Acid (B1): **B1** was prepared using a literature procedure and obtained as a red solid.[15] Yield 13.5%. ^{1}H NMR (500 MHz, $CDCl_3$): δ 8.27 (d, *J* = 8.2 Hz, 2H), 7.48 (d, *J* = 8.2 Hz, 2H), 6.02 (s, 2H), 2.59 (s, 6H), 1.40 (s, 6H). ^{13}C NMR (126 MHz, DMSO): δ 167.30, 155.74, 143.11, 141.25, 138.89, 131.96, 130.74, 130.62, 128.87, 122.07, 14.71, 14.53.

4-(4,4-difluoro-1,3,5,7-tetramethyl-2-iodo-4-bora-3a,4a-diaza-s-indacene-8-yl)-benzoic Acid (B2): To a solution of **B1** (184 mg, 0.5 mmol) in dry CH_2Cl_2 (50 mL) was added N-iodosuccinimide (NIS, 112 mg, 0.5 mmol) under N_2 atomosphere, and the reaction mixture was allowed to stir at room temperature for 1 h. TLC analysis indicated that the disappearance of spots corresponds to **B1** and appearance of a new spot corresponds to compound **B2**. The solvent was removed on a rotary evaporator under reduced pressure, and the resultant crude product was purified by silica gel column chromatography (CH_2Cl_2/MeOH = 30:1, v/v). The second red band was collected to give the product as a red solid in 64.8% (0.16 g). ^{1}H NMR (500 MHz, DMSO-d^6): δ 8.12 (d, J = 8.3 Hz, 2H), 7.55 (d, J = 8.3 Hz, 2H), 6.32 (s, 1H), 2.54 (d, J = 15.8 Hz, 3H), 2.48 (d, J = 16.2 Hz, 3H), 1.33 (d, J = 4.7 Hz, 6H). ^{13}C NMR (126 MHz, DMSO): δ 167.24, 158.64, 154.18, 145.46, 142.83, 141.07, 138.70, 132.15, 131.40, 130.71, 128.86, 123.38, 85.84, 16.78, 16.00 14.94, 14.76. Anal. Cacld for $C_{20}H_{18}BF_2IN_2O_2$: C, 48.62; H, 3.67; N, 5.67. Found: C, 48.75; H, 3.78; N, 5.80.

4-(4,4-difluoro-1,3,5,7-tetramethyl-2,6-diiodo-4-bora-3a,4a-diaza-s-indacene-8-yl)-benzoic Acid (B3): **B3** was prepared using a literature procedure and obtained as a deep red solid.[1] Yield: 90%. ^{1}H NMR (500 MHz, $CDCl_3$): δ 8.31 (d, J = 8.2 Hz, 2H), 7.46 (d, J = 8.1 Hz, 2H), 2.68 (s, 6H), 1.41 (s, 6H). ^{13}C NMR (126 MHz, $CDCl_3$): δ 169.61, 157.55, 145.04, 140.44, 131.24, 130.26, 128.49, 85.97, 17.18, 16.12.

2-(4,4-difluoro-1,3,5,7-tetramethyl-4-bora-3a,4a-diaza-s-indacene-8-yl)-benzoic Acid (B4): **B4** was prepared using a literature procedure and obtained as a red solid.[16] Yield 25%. ^{1}H NMR (500 MHz, DMSO): δ 8.05 (dd, J = 7.8Hz, 1H), 7.77 (dd, J = 7.5, 1.2 Hz, 1H), 7.68 (dd, J = 7.7, 1.2 Hz, 1H), 7.40 (dd, J = 7.6, 1H), 6.14 (s, 2H), 2.45 (s, 6H), 1.29 (s, 6H). ^{13}C NMR (126 MHz, DMSO): δ 167.26, 154.44, 143.03, 142.16, 135.06, 133.49, 131.50, 131.16,131.04, 130.20, 129.74, 121.47 , 14.64, 14.04.

2-(4,4-difluoro-1,3,5,7-tetramethyl-2,6-diiodo-4-bora-3a,4a-diaza-s-indacene-8-yl)-benzoic Acid (B5): To a solution of **B4** (184 mg, 0.5 mmol) in dry CH_2Cl_2 (30 mL) was added an excess of NIS (448 mg, 2 mmol), and the mixture was stirred at room temperature for about 30 min (monitored by TLC until complete consumption of the starting material). The reaction solution was concentrated under vacuum, and the crude product was purified by silica-gel column chromatography (Hexane/EtOAc/MeOH = 100:30:3, v/v/v), affording a deep red solid in 74.3% (0.23 g). ^{1}H NMR (500 MHz, $CDCl_3$): δ 8.27 (dd, J = 7.8Hz, 1H), 7.76 (dd, J = 7.5, 1.2 Hz, 1H), 7.67 (dd, J = 7.7, 1.2 Hz, 1H), 7.34 (dd, J = 7.6, 1H), 2.67 (s, 6H), 1.34 (s, 6H). ^{13}C NMR (126 MHz, $CDCl_3$): δ 168.35, 156.41, 144.16, 141.09, 136.59, 134.10, 132.18, 130.94, 129.96, 129.65, 128.88, 85.54, 16.60, 16.06. Anal. Cacld for $C_{20}H_{17}BF_2I_2N_2O_2$: C, 38.75; H, 2.76; N, 4.52. Found: C, 38.85; H, 2.84; N, 4.70.

4,4-difluoro-8-phenyl-1,3,5,7-tetramethyl-4-bora-3a,4a-diaza-s-indacene (B6): **B6** was prepared using a literature procedure and obtained as an orange solid.[17] Yield 72%. ^{1}H NMR (500 MHz, $CDCl_3$): δ 7.62-7.38 (m, 3H), 7.37-7.21 (m, 2H), 6.00 (s, 2H), 2.58 (s, 6H), 1.40 (s, 6H). ^{13}C NMR (126 MHz, $CDCl_3$): δ 155.43, 143.15, 141.73, 135.00, 131.44, 129.12, 128.93, 127.94, 121.19, 14.59, 14.34.

4,4-difluoro-8-phenyl-1,3,5,7-tetramethyl-2,6-diiodo-4-bora-3a,4a-diaza-s-indacene (B7): **B7** was prepared using a literature procedure and obtained as a red solid.[18] Yield 84%. ^{1}H NMR (500 MHz, $CDCl_3$): δ 7.58-7.50 (m, 3H), 7.28 (dd, *J* = 6.6, 3.2 Hz, 2H), 2.67 (s, 6H), 1.41 (s, 6H). ^{13}C NMR (126 MHz, $CDCl_3$): δ 156.77, 145.37, 141.37, 134.73, 131.30, 129.50, 127.77, 85.68, 16.96, 16.00.

4,4-difluoro-8-(4-(methoxycarbonyl)phenyl)-1,3,5,7-tetramethyl-4-bora-3a,4a-diaza-s-indacene) (B8): **B8** was prepared using a literature procedure and obtained as a red solid.[19] Yield 23%. ^{1}H NMR (500 MHz, $CDCl_3$): δ 8.20 (d, J = 8.3 Hz, 2H), 7.42 (d, J = 8.3 Hz, 2H), 6.01 (s, 2H), 3.99 (s, 3H), 2.58 (s, 6H), 1.37 (s, 6H). ^{13}C NMR (126 MHz, $CDCl_3$): δ 166.47, 155.99, 142.89, 140.22, 139.83, 130.81, 130.37, 128.38, 121.50, 52.40, 14.62, 14.50.

4,4-difluoro-8-(4-(methoxycarbonyl)phenyl)-1,3,5,7-tetramethyl-2,6-diiodo-4-bora-3a,4a-diaza-s-inda-cene) (B9): **B9** was prepared using a literature procedure and obtained as a

red solid.[19] Yield 86%. ^{1}H NMR (500 MHz, $CDCl_3$): δ 8.23 (d, J = 8.3 Hz, 2H), 7.40 (d, J = 8.3 Hz, 2H), 4.01 (s, 3H), 2.67 (s, 6H), 1.39 (s, 6H). ^{13}C NMR (126 MHz, $CDCl_3$): δ 166.24, 157.35, 145.07, 139.80, 139.46, 131.34, 130.80, 130.65, 128.23, 85.99, 52.52, 17.14, 16.09.

Cobaloximes **C1**-**C4** were prepared according to the literature methods.[20-21]

2.4. X-ray crystallographic analysis

Single crystals of **B1**, **B3** and **B9** suitable for X-ray diffraction analysis were obtained by slow crystallization in $MeOH/CH_2Cl_2$ at room temperature.

Single crystal X-ray data collection was carried out on a Rigaku R-AXIS RAPID Image Plate single-crystal diffractometer at room temperature using Mo K_α radiation (λ = 0.71073 Å), monochromatised by a graphite crystal. Absorption correction was applied by correction of symmetry-equivalent reflections using the ABSCOR program.[22] All structures were solved by direct methods using SHELXS-97[23] and refined by full-matrix least-squares on F^2 using SHELXL-97[24] via the program interface X-Seed.[25] All non-hydrogen atoms were refined with anisotropic displacement parameters. Hydrogen atoms attached to oxygen in **B1** and **B3** were located by difference Fourier maps and other hydrogen atoms were placed in ideal positions and refined as riding atoms with U_{iso} values 1.2-1.5 times those of their parent atoms. All structures were examined using the Addsym subroutine PLATON[26] to ensure that no additional symmetry could be applied to the models. Crystal structure views were obtained using Diamond v3.1.[27] A summary of crystallographic data for these three compounds is included in the Supporting Information as Table S1 and in CIF format. CCDC reference numbers: 1045034-1045036.

2.5. Photolysis reactions

The photocatalytic water splitting experiment was performed in a Pyrex top-irradiation reaction vessel connected to a glass closed gas circulation system (Labsolar-IIIAG photocatalytic system, Beijing Perfectlight Co., Ltd., Fig. S1 of ESI†). In a typical homogeneous hydrogen production experiment, solutions of a BODIPY (1.0×10^{-4} M) and a cobaloxime (2.5×10^{-4} M) were prepared in a mixture of acetonitrile-water 3:2 (v/v), containing 5 vol% of triethanolamine (TEOA) at pH = 8.5. In a typical heterogeneous hydrogen production experiment, 60 mg of 0.5 wt% Pt/TiO_2 powder was redispersed in a mixture of CH_3CN-H_2O 1:1 (v/v). The sensitizer concentration added to the suspension was 0.1 mM. 10 vol% of TEOA was added in the suspension as an electron donor. The pH of reaction system was kept at 7 with a 2.5 M HCl stock solution. Reaction solution was transferred to a 250 mL Pyrex flat-bottomed reaction vessel and vigorously stirred in the dark for 15 min. The reaction system was then freeze-pump-thaw degassed three times to remove air prior to illumination. The reaction solution was irradiated using an external light source comprising a 300 W Xe arc lamp (MICROSOLAR 300, Beijing Perfectlight Co., Ltd.) with a cut-off optical filter (λ > 420 nm). During photolysis reaction, the mixture was mixed using a magnetic stirring bar and the temperature of the reactant solution was maintained at room temperature by a flow of cooling water. The amount of H_2 gas produced in the reaction system was measured with a gas chromatograph (GC 7900, Shanghai Techcomp Instrument Ltd.) with a thermal conductivity detector (TCD), a 5 Å molecular sieve column (4 mm(OD) × 3mm(ID) × 3m), and with N_2 as carrying gas. Duplicate experiments were carried out under identical conditions to confirm the reproducibility. The hydrogen dissolved in solution was neglected. The amounts of hydrogen were quantified by external standard method, and the turnovers were calculated versus the amount of photosensitizer in the system.

2.6. Synthesis of Pt-supported TiO_2 nanoparticles (Pt/TiO_2)

Pt/TiO_2 nanoparticles were prepared by photodeposition of Pt from a H_2PtCl_6 aqueous solution onto TiO_2 with using methanol as an electron donor according to the previous work.[28] In a typical synthesis, the TiO_2 particles (0.2g, Degussa P25) were suspended in a 500 mL round-bottom flask containing 160 mL of water and 40 mL of methanol; 1.23 mL of 4.18 mM $H_2PtCl_6 \cdot 6H_2O$ aqueous solution was added to obtain a 0.5 wt% of Pt loading ($Pt/(Pt + TiO_2) \times 100\%$). The flask was then sealed and sonicated for 15 min followed by magnetic stirring under nitrogen bubbling for 1 h. Photodeposition was performed by the irradiation with a 300 W xenon lamp (PLS-SXE 300C, Beijing Perfectlight Co., Ltd.). The flask was kept in front of the lamp for 2 h with continuous stirring. Nitrogen gas was gently flowed over the headspace during the entire deposition process. The obtained Pt/TiO_2 (0.5 wt% Pt) nanoparticles were washed repeatedly with a large excess of water, and dried at 70 ºC.

2.7. Assembling of the dye-sensitized solar cell (DSSC).

The construction of the dye sensitized solar cell device requires first cleaning of the fluorine doped tin oxide (FTO) coated glass substrates in a deionized water bath, and the TiO_2 colloid paste was spread over the substrate with a doctor blading technique using adhesive tape as a spacer. The substrate was sintered at 450 °C for 30 min in air, The substrate was then put into the dye solution (0.1 mM in methanol) at room temperature and kept for 2 days to obtain better effciency. The substrate was taken out, flushed with methanol, and vacuum-dried for 1 h, a dye-sensitized TiO_2 electrode was obtained. A DSSC was assembled by filling an electrolyte solution (0.6 M tetrapropylammonium iodide, 0.1 M iodine, 0.1 M lithium iodide, 0.5 M 4-tert-butylpyridine (TBP) in acetonitrile) between the dye-sensitized TiO_2 electrode and a platinized conducting glass electrode. The two electrodes were clipped together, and a cyanoacrylate adhesive was used as sealant to prevent the electrolyte solution from leaking.

2.8. Photovoltaic and EIS measurements

The photovoltaic test of DSSC was carried out by measuring the current-voltage (*J-V*) characteristic responses under irradiation of white light from a 100 W xenon arc lamp (XQ-500W, Shanghai Photoelectricity Device Company, China) in ambient atmosphere. The fill factor (*FF*) and the overall light-to-electrical energy conversion efficiency (*η*) of DSSC were calculated according to the following equations[29]:

$$FF = \frac{V_{\max} \times J_{\max}}{V_{oc} \times J_{sc}} \quad (1)$$

$$\eta(\%) = \frac{V_{\max} \times J_{\max}}{P_{in}} \times 100\% = \frac{V_{oc} \times J_{sc}}{P_{in}} \times 100\% \quad (2)$$

where J_{SC} is the short-circuit current density (mA·cm^{-2}), V_{OC} is the open-circuit voltage (V), Pin is the incident light power, and J_{max} (mA·cm^{-2}) and V_{max} (V) are the current density and voltage at the point of maximum power output on the *J-V* curves, respectively.

Electrochemical impedance spectroscopy (EIS) measurements were performed in dark under forward bias -0.5 V. A simplified Randle's model was used to fit the data to extract the series resistance (R_S), which accounts for the transport resistance of FTO, the combined charge transfer resistance for electron recombination at the FTO/electrolyte and TiO_2/electrolyte interface (R_{ct}).

2.9. Quantum chemical calculations

All the quantum-chemical calculations were performed using the Gaussian 09 package.[30] For the purpose of accordance with experiment results, the geometric parameters taken from X-ray diffraction analysis were used as the starting point for the geometry optimization when available. Ground-state geometries were fully optimized under the density functional theory (DFT) using the hybrid functional B3LYP, which combines Becke's 3-parameter exchange functional[31] and Lee, Yang, and Parr's correlation functional.[32] The polarizable continuum model (PCM)[33] in methanol solvent was employed in all calculations. The BODIPY chromophores were optimized using the 6-31+G(d) basis set,[34] excluding the iodinated compounds, for which 3-21G[35] was used for iodine atoms while the 6-31+G(d) was used for the remaining atoms. All geometries were deemed minima, as no negative frequencies were found. Time-dependent density functional theory (TDDFT)[36] has been applied to compute the vertical transition energies. The contours of the HOMO and LUMO orbitals of **B1**-**B5**, **B3**$^{+\bullet}$, **B3**$^{-\bullet}$ were plotted using the software Gaussview 5.0.

3. Results and discussion

3.1. Synthesis and crystal structures

Meso-aryl substituted BODIPY derivatives of **B1**, **B4**, **B6** and **B8** were achieved in a facile three-step one-pot procedure often used for the synthesis of BODIPY dye which allows a straightforward preparation of several hundreds milligrams of the desired compounds. Briefly, two 2,4-dimethylpyrrole units were condensed with the aryl aldehyde under catalytic conditions of trifluoroacetic acid (TFA), followed by oxidation with 2,3-di-chloro-5,6-dicyanobenzoquinone (DDQ) and chelation with $BF_3{\cdot}OEt_2$ in the presence of triethylamine (TEA). Following work-up, the BODIPYs were purified by silica gel column chromatography and recrystallized, to give the target compounds in ~15% to 60% yields. Further iodination of **B1**, **B4**, **B6** and **B8** affords **B2**, **B3**, **B5**, **B7** and **B9**, which was accomplished through electrophilic substitution at the 2-position or 2,6-positions using iodic acid with excellent yields (~60-90%). All BODIPY compounds were characterized by ^{1}H and ^{13}C NMR, and in the case of **B1**, **B3** and **B9** by X-ray crystallography. A more detailed description of the synthesis and the analytical characterization is given in the Experimental Section. These *meso*-aryl BODIPYs were synthesized to investigate the effect of iodination and varying the position of –COOH substituent groups on the photogeneration of H_2 and photocurrent generated upon visible light irradiation.

Single crystals of **B1**, **B3** and **B9** suitable for X-ray diffraction analysis were obtained by slow evaporation of their CH_2Cl_2-hexane solution. X-ray diffraction analysis reveals all these compounds crystallize in the same triclinic *P*-1 space group. The crystal data of these compounds are listed in Table S1 and in CIF format. Thermal ellipsoid drawings of **B1**, **B3** and **B9** are shown in Fig. 1. The structure of **B1** shows that the two pyrrole rings and the central six-membered ring containing the boron atom are in one plane like any other BODIPY,[37] with the very small maximum deviation from the least-squares mean plane of the C_9BN_2 (12-atom) frame being 0.012. For **B3** or **B9**, despite the introduction of two iodine atoms onto the sensitizer **B1**, the planarity of the central 12-atom core was still preserved. The root-mean-square (rms) deviation from planarity is 0.014 Å for **B3**, and 0.016 Å for **B9**, respectively. This lends weight to the supposition that introduction of the iodines at the *β*-pyrrole positions of **B1** could give rise to a more efficient population of the triplet state without causing an increase in nonradiative decay to the ground state. Two methyl substituents attached at C-1 and C-7 positions of BODIPY moiety in **B1**, **B3** and **B9** were revealed to prevent the free rotation of *meso*-aryl moiety, resulting in an almost perpendicular configuration between the *meso*-aryl and BODIPY moieties with the dihedral angle being 84.3º for **B1**, 82.77º for **B3**, and 83.77º for **B9**.

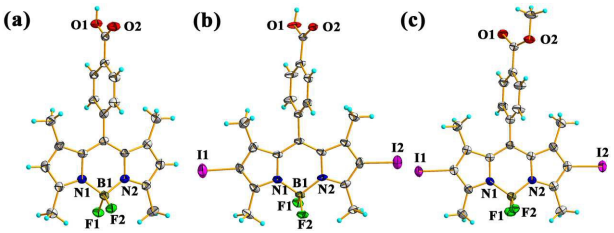

Fig. 1 ORTEP diagram of BODIPY derivates **B1** (a), **B3** (b), and **B9** (c). Thermal ellipsoids are drawn at the 50% probability level.

3.2. Photophysical properties, theoretical calculations and electrochemical studies

A series of BODIPY derivatives (**B1**-**B5**) were measured in methanol solution via UV-vis absorption and steady-state fluorescence spectroscopy, and the data are summarized in Table 1. The absorption spectrum of **B1** with a *para*-carboxyl group is of comparable shape as those of described BODIPY dyes,[37] with an intense absorption band centered at ~498 nm, ascribed to the $S_0 \rightarrow S_1$ ($\pi \rightarrow \pi^*$) transition of the BODIPY moiety. It is observed that stepwise introduction of iodines at the pyrrole carbons of the BODIPY core in **B2** and **B3** showed $S_0 \rightarrow S_1$ transition which experienced a bathochromic shift of 13-23 nm compared to that of unsubstituted **B1**. The bathochromic electronic transitions observed are consistent with the calculated reduced HOMO-LUMO gaps by the following Density functional theory (DFT) computational studies. The spectral bandwidth of the principal absorption band can be analyzed by the full width at half-maximum (*fwhm*) values, which vary from 20 to 30 nm in methanol. This sharp absorption band is

indicative of a nonaggregated system in these solutions. The fluorescence emission spectra of **B1**-**B3** in methanol were mirror images of the absorbance spectra with Stoke shifts in the range of 10-17 nm, indicating small change in the dipole moment between the ground and excited state of BODIPY moiety in these three compounds. Also, there was no evidence for aggregation for these compounds in solution, as the shape and normalized intensity of the photoluminescence spectra did not vary as a function of dye concentration. **B1** showed a moderate fluorescence quantum yield (Φ_{fl}) determined as ~0.44 in methanol. For the mono-iodine substituted **B2**, the Φ_{fl} decreases to ~0.1. In comparision, the introduction of two iodine atoms into the core of BODIPY gave rise to substantial reduction fluorescence quantum yield (Φ_{fl} = 0.02) for **B3**. The fluorescence decay profiles of **B2** and **B3** which could be described by a single-exponential fit (fluorescence lifetimes τ_{fl} of 0.77-2.80 ns) obviously reduced when compared to **B1** (τ_{fl} = 3.33 ns). Significant decrease of Φ_{fl} and τ_{fl} indicates that the presence of I atoms facilitates an efficient intersystem crossing efficiency (Φ_{ISC}) from the lowest singlet excited state to the triplet states, which results in population of the longer lived triplet excited states from which electron transfer occurs. When compared with **B1**, **B4** with –COOH positioned at *ortho*-position, shared a similar absorption and emission profile, but augmented the absorption (ε = 91000 M^{-1} cm^{-1} for **B4** *vs*. ε = 86000 M^{-1} cm^{-1} for **B1**), and fluorescence (Φ_{fl} = 0.89 and τ_{fl} = 7.06 ns for **B4**) significantly. Upon iodination of two pyrrole 2,6-positions, both the absorption and emission maxima of **B5** shift to lower energy. The measured Φ_{fl} and τ_{fl} decreasing markedly to 0.03 and 0.76 ns in CH_3OH are similar to those determined for **B3**, which reflects the heavy atom effect of the iodide-atoms increasing spin-orbit coupling, compared to the corresponding precursor **B4**.

DFT has proved suitable for calculating the electronic distribution and molecular orbitals of a series of BODIPY derivatives.[37,38] The calculations with the effect of the environment included through the polarizable continuum model (PCM) were performed to gain deeper insight into the structural geometries and nature of the transitions involved in the lowest energy states of the BODIPYs (**B1**-**B5**) from the optimized geometries. The parameters for the optimized geometries and full list of excited states are included in the Supporting Information. The energy gap between the highest occupied molecular orbitals (HOMO) and the the lowest occupied molecular orbitals (LUMO) does not change with varying the position of carboxyl group from *ortho*-position to *para*-position and is found to be 2.99 and 3.00 eV for **B1** and **B4**, respectively. However, after introducing two iodine atoms onto the C-2 and C-6 positions, both the HOMO and LUMO energies of bis-iodo-BODIPYs **B3** and **B5** become evidently higher in comparision with those of corresponding counterparts in noniodinated **B1** and **B4**, namely **B3** > **B1**, and **B5** > **B4**. However, the HOMO level for **B3** and **B5** increases to a larger extent than the corresponding LUMO level, leading to a greater narrowing of the HOMO-LUMO gap for **B3** and **B5** relative to **B1** and **B4**. The HOMO-LUMO gaps (band gaps) for iodo-substituted **B3** and **B5** were calculated to be 0.96 and 0.88 eV, respectively, which is responsible for a redshift in the wavelength observed for the main absorption band. Both the contours of the electronic distribution in HOMO and LUMO states of these BODIPYs (**B1**-**B5**) are located almost on the BODIPY moiety. The localized FMOs (frontier molecular orbitals) of these BODIPYs indicate the absence of any significant electronic conjugation between the BODIPY moieties and *meso*-aryl groups. It is postulated that the nearly pure HOMO-LUMO electron transition corresponds to the emissive $S_0 \rightarrow S_1$ ($\pi \rightarrow \pi^*$) excited state in these compounds, as observed in other BODIPY derivatives reported previously.[8,37] The time-dependent DFT (TDDFT) calculation shows a lowest energy singlet transition of HOMO→LUMO character with a high oscillator strength (0.55-0.58) and energy (2.67-2.87 eV). Although the energy of the predicted BODIPY-based transition is much higher than that of the observed experimental values, TDDFT calculations are known to overestimate the excitation energy of BODIPY chromophores.[39] The compounds **B2**, **B3** and **B5** were hypothesized to enable the formation of the triplet excited state by ISC as iodine atoms are introduced into the cores of BODIPYs. The HOMO(π)-LUMO(π^*) transition corresponds to the first singlet excitation as assigned by TDDFT, which is observed in other BODIPY derivatives.[37] In each iodinated BODIPY, the nature of the HOMO and LUMO is unchanged upon iodization (Scheme S1 of ESI†). The computed similarity between these FMO orbitals indicates that, apart from its influence on the rate of ISC, iodination exerts negligible change on the electronic structures of the BODIPYs. In addition, the calculated singlet-triplet state energy gap (ΔE) of iodinated BODIPYs is small (ΔE = 0.18, 0.01, and 0.02 eV for **B2**, **B3** and **B5**, respectively), indicating the use of a iodinated BODIPY dye triplet state involves a relatively small energy loss.

The redox behaviors of the BODIPY dyes **Bn** (n = 1-5) were further studied by cyclic voltammetry in dry acetonitrile using tetrabutylammonium hexafluorophosphate (TBAP) as a supporting electrolyte, and the electrochemical data are gathered in Table 1. Within the electrochemical window of CH_3CN, all these BODIPY compounds exhibited one-electron oxidation and reduction, which are attributed to removal from or addition of one electron to the FMOs of **B1**-**B5**. Compared to non-iodinating BODIPYs (**B1** and **B4**), BODIPYs with one or two iodo atoms on the 2-position or 2,6-positions (**B2**, **B3**, and **B5**) appeared less negative reduction and more positive oxidation potentials, indicating that iodinated compounds (**B2**, **B3** and **B5**) are easier to get one electron to be reduced than the corresponding counterparts (**B1** and **B4**). This supports the electron-deficient nature of iodo-substituted BODIPYs due to the presence of iodine atoms at the core of the pyrrole, which is consistent with the foregoing results of DFT calculations. In addition, comparison of the redox behaviours between the *para*-carboxyl substituted BODIPYs (**B1** and **B3**) and *ortho*-carboxyl substituted BODIPYs (**B4** and **B5**), namely **B1** *vs*. **B4** (0.80 V *vs*. 0.75 V, -1.58 V *vs*. -1.62 V) and **B3** *vs*. **B5** (0.95 V *vs*. 0.95 V, -1.31 V *vs*. -1.32 V), reveals that the position of carboxyl

anchoring unit has little electron effect on the redox activities of the central BODIPY core.

Table 1 Electrochemical and photophysical properties of dyes **B1-B5**

BODIPY	Cyclic voltammetry[a]		absorption[b]	fluorescence		
	Ox. (V)	Red. (V)	λ_{max} abs (nm) ε (M^{-1} cm^{-1})	λ_{em}[c] (nm)	Φ_{fl}[d] (%)	τ_{fl}[e] (ns)
B1	0.80	-1.58	498 (86000)	511	0.44	3.33
B2	0.86	-1.44	510 (70100)	521	0.10	2.60
B3	0.95	-1.31	531 (75600)	548	0.02	0.77
B4	0.75	-1.65	499 (91000)	511	0.89	7.06
B5	0.95	-1.32	529 (84200)	547	0.03	0.76

[a]Potentials determined by cyclic voltammetry in deoxygenated CH_3CN solution, containing 0.1 M TBAP as the supporting electrolyte recorded at 100 mV s^{-1} scan speed, at a solute concentration of *ca*. 1.0 mM and at room temperature. Potentials were standardized versus ferrocene (F_c) as internal reference. [b]λ_{max} abs (nm): absorption wavelength (at the maximum intensity), ε (M^{-1} cm^{-1}): molar extinction coefficient. [c]λ_{em} (nm): emission wavelength (at the maximum intensity). [d]Φ_{fl} (%): the fluorescence quantum yields of **B1** and **B4** were estimated with 1,3,5,7-tetramethyl-8-phenyl-BODIPY as a standard (Φ_{fl} = 0.72 in tetrahydrofuran); the fluorescence quantum yields of **B2**, **B3** and **B5** were estimated with Rhodamine B (0.49 in ethanol). [e]τ (ns): fluorescence lifetimes.

3.3. Photocatalytic hydrogen evolution in aqueous solution

3.3.1 Homogeneous photocatalytic hydrogen evolution

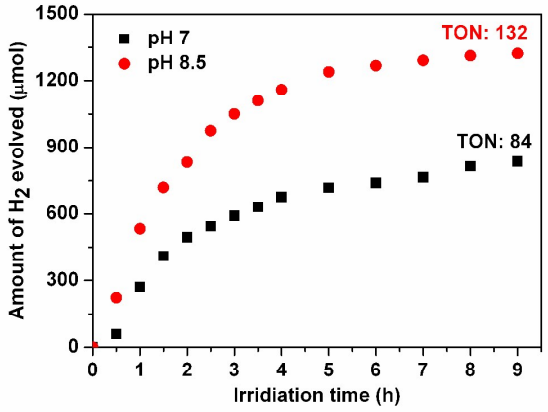

Fig. 2 Plots of hydrogen production upon irradiation (λ > 420 nm) at two different pH values of systems containing **B3** (1.0×10^{-4} M), **C1** (2.5×10^{-4} M) and TEOA (5%, v/v) in CH_3CN-H_2O (3:2, v/v).

The light-driven hydrogen generation containing BODIPYs and cobaloximes in homogeneous systems was initially studied. The hydrogen evolving performance of BODIPYs was found to be strongly dependent on initial system pH and these pH values were selected on the basis of observations in related photocatalysis systems.[7,37b] The photochemical H_2 production experiment involving **B3** as the photosensitizer, **C1** as the H_2-evolution catalyst and TEOA as sacrificial electron donor using a Xe lamp (300 W) with a cutoff filter (λ > 420 nm), was carried out at room temperature, which showed their maximum rate of hydrogen production at neutral to slightly basis pH values (7 < pH < 8.5). Fig. 2 shows the effect of pH value of the solution (pH = 7 and 8.5) on the amount of hydrogen evolution. Control photocatalytic experiments at solution pH 7 and 8.5 showed that the presence of all three components (**B3**, **C1** and TEOA) is necessary in order to observe H_2 production. It was found that activity for H_2 evolution increased with the increase of the pH value from 7 to 8.5. Cessation of hydrogen production coincides with bleaching of the photolysis solutions. To regenerate the catalytic activity of the system, addition of both **B3** and **C1** is necessary, suggesting that both the photosensitizer and the catalyst undergo at least partial decomposition in the course of the reaction.[7] Photolysis experiments performed under identical conditions but in the presence of mercury, in order to suppress any heterogeneous catalytic sites, show no appreciable change in the hydrogen production rate confirming that catalysis is of truly homogeneous nature.[40]

There is no significant change in the redox potentials for the Co^{II}/Co^{I} couple between complexes **C1-C3** in which the axial pyridine ligand is modified in the 4-position to possess either an electron-withdrawing group (-COOH) as in **C2** or an electron-donating group ($-NMe_2$) as in **C3**.[41] These catalysts (**C1-C3**) exhibit similar photocatalytic activities for hydrogen evolution with TONs of 126-131 (Fig. 3). The Co^{II}-based **C4** possessing good air and acid stability, has shown highly efficient electrocatalytic hydrogen evolution in nonaqueous media.[42] Therefore, it was also tested as a catalyst for H_2 generation under the same conditions. At pH 8.5, only a relatively modest amount of H_2 was produced (~75 TONs) after 5h of irradiation. The considerably slower rate and TONs of H_2 production with **C4**, can possibly be attributed to the more positive reduction potential of Co^{II}/Co^{I} compared to that of **C1-C3**.[41]

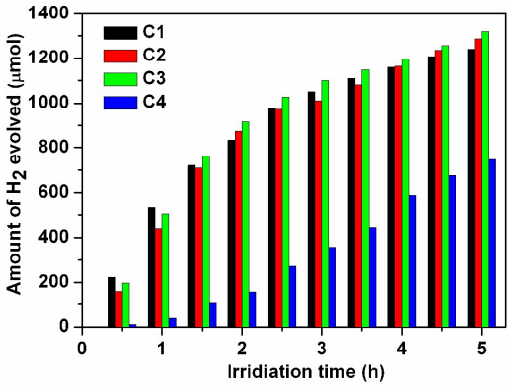

Fig. 3 Hydrogen production upon irradiation (λ > 420 nm) from the systems comprising **B3** (1.0×10^{-4} M), and a cobaloxime catalyst (2.5×10^{-4} M) and TEOA (5%, v/v) in CH_3CN-H_2O (3:2, v/v) at pH 8.5.

B1-B5 were investigated as to their effectiveness under similar experimental conditions with 100 mL of CH_3CN/H_2O (4:1, v/v) containing 2.5×10^{-4} M **C1**, TEOA (5%, v/v) combined in a 250 mL Pyrex flat-bottomed flask vigorously agitated with a magnetic stirrer. The pH of reaction system was kept at 8.5 with a 2.5 M HCl stock solution. Fig. 4 shows the time dependence of hydrogen production in this reaction system for the different BODIPY chromophores. The plot demonstrates: (i) the maximum TONs of hydrogen generation follow the order **B5** > **B3** > **B2**. H_2 evolution levels off after 5 h irradiation, with the total turnover of H_2 reached 197 (1975 μmol) for **B5** under optimal conditions, while **B3** and **B2** gave 126 (1268 μmol) and

77 (765 μmol) TONs of H_2 evolution in 5 h irradiation. Since the redox potentials and fluorescent spectra of these iodo-substituted BODIPY dyes are similar, the photocatalytic activity of H_2 generation for **B2**, **B3** and **B5** may lie with the molar extinction coefficient (ε) and quantum yield of intersystem crossing (Φ_{ISC}) of photosensitizers. Taking account of quantum yield of intersystem crossing for **B2**, **B3** and **B5** being 0.90-0.98 (Φ_{ISC} = 1- Φ_{fl}) using Amolev's rule,[43] it is amazing that there is a good correlation of $\varepsilon \times \Phi_{ISC}$ *versus* TONs of H_2 production for these iodinated BODIPYs (Fig. 5).

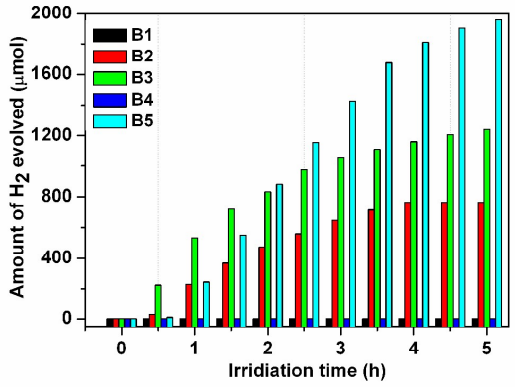

Fig. 4 Hydrogen production *vs*. PSs **B1**-**B5** obtained in the photocatalytic reaction with continuous irradiation (λ > 420 nm). Reaction composition: CH_3CN-H_2O (3:2, v/v) at pH 8.5 containing a BODIPY sensitizer (1.0×10^{-4} M), **C1** (2.5×10^{-4} M) and TEOA (5%, v/v).

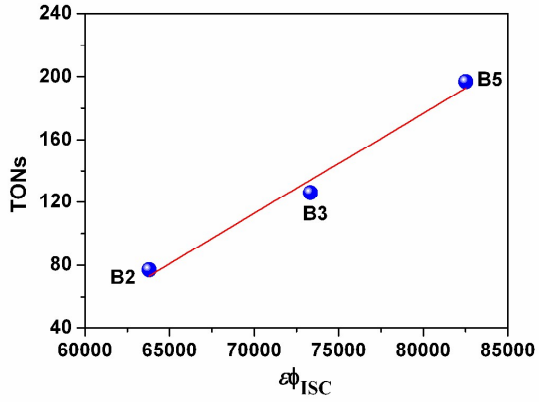

Fig. 5 A good correlation of $\varepsilon \times \Phi_{ISC}$ *versus* TONs of H_2 production for iodinated BODIPYs (**B2**, **B3** and **B5**).

An interesting observation is that when substituent groups with electron-withdrawing or donating groups lie at the *ortho*-position of phenyl ring at the 8-position on the BODIPY core, higher hydrogen production activities for the homogeneous system were found relative to other positions. At present, we temporarily call it as "*ortho*-position effect". Though we are still unclear about the reason, similar results can be found in *meso*-methylpyridyl substituted BODIPYs[44] and *meso*-pyridine-substitution BODIPYs[45], respectively. Interestingly, we observed that the carboxyl groups in the halogenated xanthene dyes Rose Bengal and Eosin Y were also located at the *ortho*-position of *meso*-phenyl ring.[7b] (ii) No observable amount of H_2 production was detected by GC for **B1** and **B4**. Compared with core-iodinated dyes **B2**, **B3** and **B5**, noniodinated **B1** and **B4** lack any appreciable hydrogen evolution under the same reaction conditions due to the absence of internal heavy atom effect and long-lived photoexcited triplet state. The S_1 excited state is unable to make hydrogen production due to the following reasons: Intermolecular electron transfer should ideally be diffusion-controlled. The short life-time (τ_{fl} = 3.33 and 7.06 ns in MeOH for **B1** and **B4**) of the singlet excited state is not favorable for being quenched *via* an intermolecular manner. The reason is that the diffusion-controlled bimolecular collision frequency (k_0) in fluid solution is *ca*. 10^9-10^{10} M^{-1} s^{-1}. As a result, the Stern-Volmer quenching constant ($K_{sv} = k_q \times \tau_0$, where k_q is the bimolecular quenching constant and τ_0 is the lifetime of the excited state of the photosensitizer) will be on the scale of 1-10 M^{-1}, which is too small to induce any efficient intermolecular electron transfer; In contrast, the excited triplet state tends to have a longer lifetime (in μs to ms), as compared with the excited singlet state (in ns). Hence, intermolecular electron transfer is possible with a triplet excited state and it is crucial for the photosensitizer to undergo rapid ISC to produce the triplet state. Although the triplet lifetimes for **B3** and **B5** were not measured due to our instrumental limitation, the analog of **B9**, not having the –COOH substituent, has a reported triplet excited-state lifetime, τ_T of 57.1 μs in MeCN,[43] which is > 30000-fold longer than the corresponding singlet excited state.

The redox potentials of photosensitizers **Bn** (n = 2, 3 and 5) are adopted to evaluate the thermodynamic driving force of the intermolecular electron transfer reactions. According to the reduction potentials of **B3** and **B5**, the ground-state redox potentials of **B3** ($E_{1/2}$ ($\mathbf{B3}^{\bullet+}$/**B3** = 0.95 V and $E_{1/2}$($\mathbf{B3}^{\bullet-}$/**B3**) = -1.31 V) and **B5** ($E_{1/2}$ ($\mathbf{B5}^{\bullet+}$/**B5** = 0.95 V and $E_{1/2}$($\mathbf{B5}^{\bullet-}$/**B5**) = -1.32 V), and the triplet excited state energies of $^3\mathbf{B3}^*$ (1.523 eV) and $^3\mathbf{B5}^*$ (1.552 eV) obtained from TDDFT calculations, the free-energy change (ΔG) of the reaction can be estimated according to the well-known Rehm-Weller equation (Table S2, ESI†).[46] It was found that the oxidative potential of the excited photosensitizer is too positive to reduce catalysts. Despite this, the reduction process is exergonic, and intermolecular electron transfer from reduced $\mathbf{Bn}^{\bullet-}$ (n = 2, 3 and 5) species to the cobaloximes is thermodynamically feasible, as estimated from the electrochemical and spectroscopic studies. Furthermore, DFT calculations for the system of **C1** + **B3** + TEOA also supported a full electron-transfer process from the HOMO level of $\mathbf{B3}^{\bullet-}$ radical anion to the LUMO of the cobaloxime **C1** is allowed (Scheme S2).

The possible initial electron transfer reaction pathways in the catalyst systems were first investigated by emission quenching studies. It was found that addition of TEOA or **C1** to the aqueous solution of **B3** did not have any effect on the fluorescence emission intensity of the singlet excited state ($^1\mathbf{B3}^*$), suggesting that $^1\mathbf{B3}^*$ does not take part in the electron transfer reaction (Fig. S2). Electron transfer quenching of the triplet excited state ($^3\mathbf{B3}^*$) can be either oxidative or reductive in the present of electron donor TEOA, leading respectively to the

formation of $\mathbf{B3}^{\bullet+}$ in which $^3\mathbf{B3}^*$ transfers an electron to the H_2 generating catalyst or $\mathbf{B3}^{\bullet-}$ in which $^3\mathbf{B3}^*$ is initially reduced by TEOA. To discriminate these two routes of electron transfer quenching through experiments and further gain a mechanistic understanding of H_2 generation by the system composed of **C1** + **B3** + TEOA, absorption spectra were acquired both pH 8.5 and 12 (Fig. S3). Before irradiation, the absorption spectra are simply the sums of the individual components. Upon irradiation (λ > 420 nm) at pH 8.5 under H_2 generating conditions, the formation of Co^{II} occurs within 2 min for **C1** + **B3** + TEOA system as evidenced by the appearance of the characteristic absorption at ~ 450 nm.[47] A change in the **B3** absorption at pH 12 is also seen suggestive of photodecomposition of **B3**, possibly by C-I cleavage from the reduced **B3**. In addition, UV-vis absorption spectra of photolysis solutions were also measured for the system of **C4** + **B3** + TEOA (Fig. 6). There is no change in the spectrum was observed on **C4** + **B3** system after 30 min irradiation, which suggests that it is negligible for the oxidative quenching of the $^3\mathbf{B3}^*$. This is further supported by the fact that, under irradiation, there was no H_2 production for the **C4** + **B3** system. The absorption spectra of the irradiated **C4** + **B3** + TEOA solution show a lower energy absorption observed at ~ 650 nm and generate the blue color characteristic due to the accumulation of a Co^I species.[47] Therefore, all these observations indicate that the electron transfer quenching of the $^3\mathbf{B3}^*$ is expected to occur through a reductive quenching mechanism only, which is consistent with the above-mentioned results of the free-energy change (ΔG) estimated by Rehm-Well equation and DFT calculations.

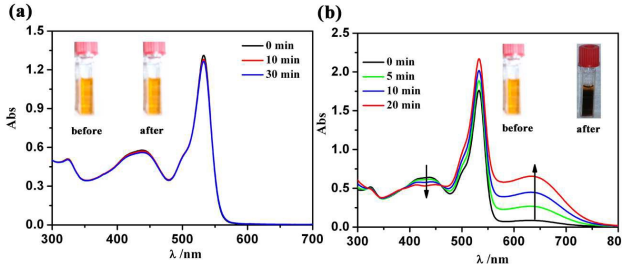

Fig. 6 (a) UV-Vis spectra at pH 8.5 before and after irradiation of a degassed solution (3:2 acetonitrile-water) containing **B3** (1.0×10^{-4} M), **C4** (2.5×10^{-4} M); Inset shows photographs of solution before and after irradiation. (b) UV-Vis spectra at pH 8.5 before and after irradiation of a degassed solution (3:2 acetonitrile-water) containing **B3** (1.0×10^{-4} M), **C4** (2.5×10^{-4} M) and TEOA (5%, v/v); Inset shows photographs of solution before and after visible light irradiation.

On the basis of the above theoretical and spectroscopic analyses, a plausible pathway of the photogeneration of H_2 is put forth as in Scheme S3. The first step is reductive quenching of the $^3\mathbf{B3}^*$ produced after ISC of the initially formed $^1\mathbf{B3}^*$ by TEOA. The next step involves the transfer the electron from $\mathbf{B3}^{\bullet-}$ to the cobaloxime. The pathway produces the radical cation of $TEOA^{+\cdot}$, which decomposes through proton loss, electron transfer and hydrolysis to form glycolaldehyde and di(ethanol)amine along with transfer of a second proton and a second electron. The formed Co^I species further reacts with a proton to produce a postulated Co^{III}-hydride, which releases molecular hydrogen via a homo- or heterolytic pathway.[41,48]

3.3.2 Heterogeneous photocatalytic hydrogen evolution

With establishment of the binding of **B1**-**B5** to TiO_2, our attention turned to using these systems for the heterogeneous photocatalytic hydrogen evolution. A noble metal Pt is usually loaded to a catalyst as a co-catalyst for heterogeneous photocatalytic water splitting, because of its high work function, low Fermi energy and the active site for hydrogen generation.[49] Pt-supported TiO_2 nanoparticles (Pt/TiO_2) were prepared using the photoreduction method. The effect of the platinum loading (wt%) on the photocatalytic activity of BODIPY-sensitized TiO_2 is first optimized and listed in Fig. 7. Control experiments in which the Pt/TiO_2 catalyst is removed produce no hydrogen. In order to determine the optimum dose of platinum the loading was varied between 0 and 0.9 wt%. The rate and TONs of hydrogen generation increased rapidly up to 0.5 wt% platinum loading. The combination of TiO_2 with the noble metal Pt will form a Schottky barrier at the metal/TiO_2 interface,[50] which is able to suppress the recombination rate of the electron/hole, and thereby, improves charge separation efficiency. Platinum metal dispersed on the TiO_2 surface basically "pumps" the photogenerated electron from TiO_2 to the absorbed species and thus hinders the possibility of their recombination with holes.[51] Additionally, platinum metal particle on TiO_2 improves reaction kinetics by decreasing the overpotential for hydrogen evolution.[52] However, with an increase in platinum content from 0.5 wt% to 0.9 wt% the photocatalytic activity for hydrogen generation was reduced. This might be ascribed to the following reasons: at higher metal loadings, the deposited metal particles may act as recombination centers rather than as separation centers for photogenerated e^-/h^+.[53]

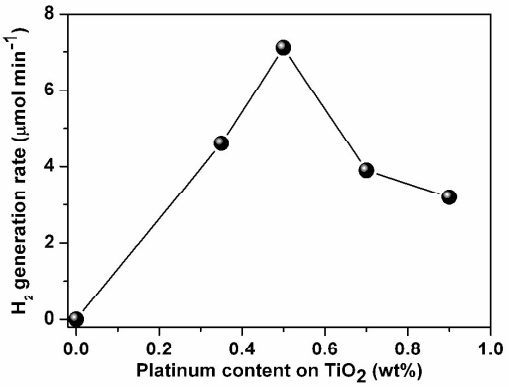

Fig. 7 Effect of Pt loading on TiO_2 on the production of H_2 in **B3**/Pt-TiO_2 suspensions. The experimental conditions were: CH_3CN-H_2O (1:1, v/v) at pH 7 containing **B3** (1.0×10^{-4} M), TEOA (10 %, v/v), Pt/TiO_2 (0.35 wt%, 0.5 wt%, 0.7 wt% and 0.9 wt%).

Solution pH value and sacrificial electron donor have a substantial effect on the photocatalytic reaction that takes place on the Pt/TiO_2 surface. This is because it will influence the existing state of the dye and electron donor reagent, and change the reduction-oxidation potential of a semiconductor. As shown in Fig. 8, the best photocatalytic activity was obtained at pH 7

in the presence of electron donor TEOA. The TONs value of hydrogen generation is ~70 after 2h irradiation ($\lambda > 420$ nm). It is apparent that a strong basic or acidic environment is disadvantageous to hydrogen production. These results can be speculated as follows. First, the pH values can influence the adsorption between BODIPY dye and TiO_2. The adsorption mode between dye and TiO_2 was similar to an este-like linkage. In the acidic solution, functional groups such as –COOH on the surface of TiO_2 were protonated by proton ions, so the ester-like linkage did not form effectively. In the strong basic solution, the carboxyl groups of BODIPY were deprotonated, so the dye could not adsorb on TiO_2 effectively because of electrostatic repulsion force. At the same time, in the basic or acidic solutions, the ester-like linkage hydrolyzes easily. Second, the pH values can also influence the existing state of the electron donor reagent, as observed in the homogeneous photocatalytic systems.

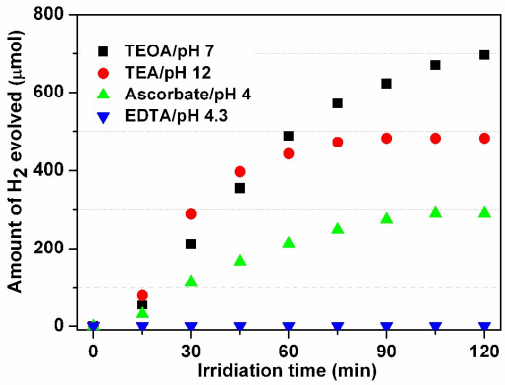

Fig. 8 Effect of initial pH and sacrificial electron donor of solutions on hydrogen production. Experimental conditions: CH_3CN-H_2O (1:1, v/v), **B3** (1.0×10^{-4} M), electron donor (10 %, v/v), Pt/TiO_2 (0.5 wt%, 60 mg).

The stability of BODIPYs sensitized Pt/TiO_2 catalyst at the optimum experimental conditions is displayed in Fig. 9, where platinized TiO_2 (Pt/TiO_2, 60 mg, Pt % = 0.5 wt %), pH = 7, TEOA and $MeCN/H_2O$ = 3:2. After 2 h visible light irradiation ($\lambda > 420$ nm), solutions containing iodinated **B2**, **B3** and **B5** produced 9, 70 and 36 TONs, respectively. Despite the modest visible light absorption, **B3** with a *para*-COOH exhibited much higher activity for the hydrogen production than **B5** with an *ortho*-COOH group. The most probable explanation appears to be related with unfavorable orientation of *ortho*-COOH group on the surface of TiO_2. Nevertheless, systems containing noniodinated **B1** or **B4** were found to make no hydrogen evolution. This result indicates the importance of iodination for photocatalytic H_2 production, as discussed in the foregoing homogeneous photocatalytic systems. It should be noteworthy that the color of the solution systems gradually turned to white after 2h irradiation, indicating the fast decomposition of dyes during the photocatalytic reaction. For the purpose of control experiments in which binding between the BODIPY photosensitizer and TiO_2 would not be expected, two other BODIPY dyes (**B7** and **B9**), were also prepared and fully characterized. The system based on **B7** that lacks any viable binding group for attachment to TiO_2 was almost inactive under visible light irradiation, whereas solutions containing **B9** only produced small amount of H_2 with TONs of ~4, indicating that there is some in situ hydrolysis of the methyl ester.

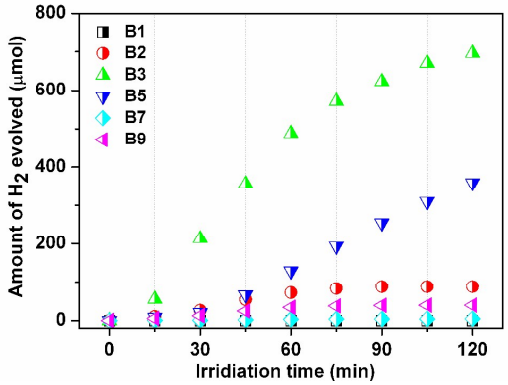

Fig. 9 Time profiles of hydrogen evolution in a visible-light-irradiated Pt/TiO_2/BODIPY suspension. Experimental conditions: CH_3CN-H_2O (1:1, v/v), **B3** (1.0×10^{-4} M), TEOA (10 %, v/v), Pt/TiO_2 (0.5 wt%, 60 mg), pH 7.

Drawing on previous studies for the mechanisms of hydrogen evolution by dye-sensitized Pt/TiO_2,[54] the proposed mechanism of photocatalytic H_2 generation in BODIPY/Pt-TiO_2 system is depicted in Fig. S4. Briefly, a certain amount of BODIPY photosensitizer (PS) might be adsorbed on the surface of platinum-loaded TiO_2. The adsorbed PS gains a photon and produces singlet excited state $^1PS^*$ upon irradiation and subsequently produce a lowest-lying triplet excited state $^3PS^*$ *via* ISC. $^3PS^*$ might be reductively quenched by TEOA to produce $PS^{\bullet-}$. Those $PS^{\bullet-}$ species might preferentially transfer their electrons into the conduction band (CB) of TiO_2. Once in the CB, these electrons are able to migrate the catalytic sites of platinum metal and effect proton reduction.

3.4. Photovoltaic performance of BODIPY-sensitized nanocrystalline TiO_2 films

Since BODIPY dyes were similarly fixed on the surface of TiO_2 through chemical anchoring groups for DSSCs and heterogeneous hydrogen production system, we expect to compare the relationship of dye structure to the effectiveness of the two systems. Immersion of nanocrystalline TiO_2 in 0.1 mM solutions of **B1**-**B5** in CH_3OH resulted in a different coloration of the films. The corresponding photovoltaic parameters are displayed in the Supplementary Information (Table S3 and Figure S6). Solar cells containing **B1**-**B5** are clearly grouped in performance according to their –COOH anchoring positions and absence or presence of iodine atoms. *para*-COOH dyes (**B1**-**B3**) exhibit the better efficiencies than *ortho*-COOH dyes (**B4**-**B5**). A similar trend was also observed for the amount of dye loading (Table S3). Relative to the *para*-COOH dyes, these *ortho*-COOH molecules will tend to occupy much of the TiO_2 surface area (Fig. S7).[55] This will heavily restrict the number of dyes that can be adsorbed onto the TiO_2 film, thereby compromising the intrinsic DSSC device performance. In addition, the poorer DSSC operational performance in the *ortho*-COOH dyes can also be rationalized in that severe charge recombination occurs

when BODIPY skeleton as an electron donor is too close to the TiO_2 semiconductor surface.[56]

The photovoltaic performance of noniodinated BODIPY **B1** with a *para*-carboxylic acid group excelled iodinated analogues (**B2** and **B3**). The same trend was also seen with the *ortho*-COOH dyes (**B4**-**B5**). The electrochemical impedance spectroscopy (EIS) measurements also show similar trend (Fig. S8). Apparently, in the DSSC, the highest efficiency obtained was **B1**, which employed both no substituent of iodine atoms and a *para*-carboxylic group. Though the device efficiency is not our concern in the current work, we would like to point out that the relatively low of BODIPY-sensitized solar cells can be primarily attributed to the relatively narrow absorption bands (not panchromatic), the strong π-stacked aggregates on the TiO_2 surface and lack of stronger donor moiety for construction of donor-(π-spacer)-acceptor (D-π-A) systems.[57]

3.5. Comparison of homogeneous and heterogeneous solar hydrogen-generating systems as well as DSSCs

No matter homogeneous or heterogeneous photoinduced hydrogen evolution systems, hydrogen production is heavily influenced by the heavy-atom iodine present in the BODIPY core, which is attributed to internal heavy atom effect for the photosensitizer's ability to undergo rapid ISC into a long-lived triplet excited state ($^3PS^*$). The $^3PS^*$ is sufficiently long-lived for bimolecular electron transfer, leading to H_2 production to be favorable relative to radiative and nonradiative decay back to the ground state. Under minimally optimized conditions, the most effective homogeneous system consisting of the photosensitizer **B5**, electron donor TEOA and catalyst **C1** has produced ~197 TONs of H_2 after 5h of photolysis with $\lambda > 420$ nm, while ~70 equivalents of H_2 per **B3** chromophore have been achieved in the heterogeneous system after 2h visible-light irradiation. It was apparent that the TONs and longevities for photocatalytic H_2 evolution from the homogeneous systems are much better than those obtained in the heterogeneous ones. The reason may be due to the followings: similar to the ruthenium bipyridyl complexes,[58] the BODIPY dyes that were bonded to the TiO_2 surface via a carboxylate linkage were not stable in water and gradually lost their activity with time. The hydrolysis of the carboxylate linkage seems to inhibit the efficient electron transfer from the BODIPY center to the CB of TiO_2.

Additionally, for the current BODIPY-based hydrogen generation homogeneous and heterogeneous systems, the photochemical quenching step of the excited-state photosensitizers (PS^*) is reductive, thus leading to unstable $PS^{\bullet-}$ radical anions that may undergo decomposition and make the system longevity for H_2 production affected. The reduced dye which is more unstable than its oxidized form can be understood in terms of HOMO and LUMO energy levels as well as HOMO-LUMO energy gaps of $PS^{\bullet+}$ and $PS^{\bullet-}$ (Table S4 and Fig. S9). In DFT calculations, there is a marked destabilization of the HOMO of $\mathbf{B3}^{\bullet-}$ relative to that of **B3**. The calculated HOMO-LUMO energy gap of $\mathbf{B3}^{\bullet-}$ is much smaller than that of $\mathbf{B3}^{\bullet+}$. The results of calculations indicate that the stability of cationic dye $\mathbf{B3}^{\bullet+}$ is stronger than that of anionic dye $\mathbf{B3}^{\bullet-}$. Thus, the development of oxidative quenching of the excited dye via electron transfer to the catalyst would be of great value for obtaining long-lived artificial photosynthesis systems.

The carboxylic anchoring groups, which enable adsorption of the dyes onto the TiO_2 nanoparticles for electron injection, are crucial for heterogeneous hydrogen generation and DSSCs, as no hydrogen and photocurrent generated when a BODIPY photosensitizer lacking a suitable linking group was used. The orientation of carboxyl anchor group also plays a vital role in the activity of light-driven hydrogen production and DSSCs. **B3** was the most efficient for the sensitized production of hydrogen among BODIPYs. In contrast to this, **B3** is the least efficient sensitizer among BODIPY dyes when they were compared for the photovoltaic performance. The distinct difference between the two systems may be ascribed to the following several key features: (i) in DSSCs, efficient charge separation takes place due to ultrafast electron injection from the singlet excited state of the dye into the conduction band of TiO_2 in the picosecond time scale.[59] Thus, noniodinated BODIPY dyes showed better overall efficiencies than iodinated BODIPYs. In comparison, slower electron transfer is crucial for efficient heterogeneous hydrogen production, making the chromophore's triplet yield an important parameter. Therefore, only the iodo-containing species forms an appreciable amount of the triplet state, which correlates well with its greater ability to generate H_2 upon irradiation. (ii) When TiO_2 films were sensitized in CH_3OH solution of BODIPY dyes, the absorption spectra were broader than those of the solution samples because of strong intermolecular interactions and aggregation (Fig. S10a).[60] In contrast to the results on TiO_2 films, aggregation does not occur when the dyes are attached to TiO_2 in a colloidal suspension in methanol, in which case the narrow absorption spectra resemble those of the solution samples (Fig. S10b). Thus the discrepancy in rates of electron transfer appears to be caused by the presence or absence of aggregation in the system, altering the coupling between the dye and TiO_2, which resembles previous reports using chalcogenorhodamine sensitizers for solar hydrogen production with a platinized TiO_2 catalyst based on transient spectroscopy observation.[54a]

4. Conclusions

As a consequence, a family of BODIPY dyes (**B1**-**B5**) with a carboxylic acid anchoring group were successfully synthesized and characterized in this work. By realizing the molecular structures of these dyes and relating them to the effectiveness of homogeneous and heterogeneous solar hydrogen evolution and DSSC device operational performance, corresponding structure-property relationships was rationalized. Comparison of homogeneous and heterogeneous photocatalytic systems shows that the properties of photochemical H_2 production have relations with the intersystem crossing efficiency accelerated through judicial heavy-atom substitution and positions of anchoring groups of optical absorbers. The longer-lived triplet state is necessary for effective electron transfer. However, photogeneration of H_2 proceeds with higher efficiency and

stability in the homogeneity than in the heterogeneity, which may be attributed to that the BODIPYs bonded to the TiO_2 surface via a carboxylate linkage were not stable in water and gradually lost their activity with time. In addition, an interesting "*ortho*-position effect" was observed in the homogeneous systems, i.e., when electron-withdrawing or donating groups were substituted at the *ortho*-position of *meso*-phenyl moiety, higher hydrogen production activities were obtained. A reaction pathway involving reductive quenching of the triplet excited state of the dye giving the reduced dye that then transfers an electron to the cobaloxime or the particulate platinized TiO_2 catalyst is proposed in the present homogeneous and heterogeneous systems. The photoreduced dye which is more unstable than its oxidized form can be understood by DFT calculations. This suggests that the development of oxidative quenching of the excited dye is preferable for obtaining long-lived photocatalytic hydrogen production systems.

Since BODIPY dyes were similarly fixed on the surface of TiO_2 electrode (DSSCs) and Pt/TiO_2 (hydrogen-generating systems) through chemical anchoring groups, one may expect to see similar behaviors between the two systems. However, the outcome is quite contrary to the expectation: **B3** was the most efficient for the dye-sensitized solar H_2 generation, but the least efficient sensitizer for the DSSC. This is because the electron-transfer rates and the degree of dye aggregation are very different in the two systems, although the same sensitizers were compared. The work reported in this paper reminds us to use caution when looking at other potential dyes for use in solar energy conversion.

Acknowledgements

We are grateful to the National Natural Science Foundation of China (21201066), the Natural Science Foundation of Fujian Province (2011J01047), the outstanding Youth Scientific Research Cultivation Plan of Colleges and Universities of Fujian Province (JA13008), and Promotion Program for Young and Middle-aged Teacher in Science and Technology Research of Huaqiao University (ZQN-PY104) for financial support of this work. We also thank the National Innovative Foundation Project for undergraduates (20140385003).

Notes and References

(1) (a) K. Sakai, H. Ozawa, *Chem. Rev*., 2007, **107**, 3032-3041. (b) S. Berardi, S. Drouet, L. Francàs, C. Gimbert-Suriñach, M. Guttentag, C. Richmond, T. Stoll, A. Llobet, *Chem. Soc. Rev*., **2014**, *43*, 7501-7519.

(2) (a) B. O'Regan, M. Grätzel, *Nature* **1991**, *353*, 737-740. (b) M. Grätzel, *Nature* **2001**, *414*, 338-344. (c) N. Anscombe, *Nature Photonics* **2011**, *5*, 266-267.

(3) (a) N. Robertson, *Angew. Chem. Int. Ed*., **2006**, *45*, 2338-2345. (b) C.Y. Chen, S.J. Wu, C.G. Wu, J.G. Chen, K.C. Ho, *Angew. Chem. Int. Ed*., **2006**, *45*, 5822-5825. (c) S. Fukuzumi, T. Kobayashi, T. Suenobu, *Angew. Chem. Int. Ed*., **2011**, *50*, 728-731. (d) W.R. McNamara, Z. Han, C.J. Yin, W.W. Brennessel, P.L. Holland, R. Eisenberg, *Proc. Natl. Acad. Sci., U. S. A*. **2012**, *109*, 15594-15599.

(4) (a) M.K. Nzeeruddin, P. Pechy, T. Renouard, S.M. Zakeeruddin, R. Humphry-Baker, P. Comte, P. Liska, L. Cevey, E. Costa, V. Shklover, L. Spiccia, G.B. Deacon, C.A. Bignozzi, M. Grätzel, *J. Am. Chem. Soc*., **2001**, *123*, 1613-1624. (b) M.K. Nzeeruddin, F.D. Angelis, S. Fantacci, A. Selloni, G. Viscardi, P. Liska, S. Ito, B. Takeru, M. Grätzel, *J. Am. Chem. Soc*., **2005**, *127*, 16835-16847. (c) J. Zhang, P.W. Du, J. Schneider, P. Jarosz, R. Eisenberg, *J. Am. Chem. Soc*., **2007**, *129*, 7726-7727.

(5) D. Heredia, J. Natera, M. Gervaldo, L. Otero, F. Fungo, C.Y. Lin, K.T. Wong, *Org. Lett*., **2010**, *12*, 12-15.

(6) (a) T. Horiuchi, H. Miura, K. Sumioka, S. Uchida, *J. Am. Chem. Soc*., **2004**, *126*, 12218-12219. (b) S. Kim, J.K. Lee, S.O. Kang, J. Ko, J.H. Yum, S. Fantacci, F. De Angelis, D. Di Censo, M.K. Nazeeruddin, M. Grätzel, *J. Am. Chem. Soc*., **2006**, *128*, 16701-16707. (c) D.P. Hagberg, T. Edvinsson, T. Marinado, G. Boschloo, A. Hagfeldt, L.C. Sun, *Chem. Commun*., **2006**, 2245-2247.

(7) (a) P. Zhang, M. Wang, J.F. Dong, X.Q. Li, F. Wang, L.Z. Wu, L.C. Sun, *J. Phys. Chem., C* **2010**, *114*, 15868-15874. (b) T. Lazarides, T.P. McCormick, W. Du, G.G. Luo, B. Lindley, R. Eisenberg, *J. Am. Chem. Soc*., **2009**, *131*, 9192-9194. (c) T.M. McCormick, B.D. Calitree, A. Orchard, N.D. Kraut, F.V. Bright, M.R. Detty, R. Eisenberg, *J. Am. Chem. Soc*., **2010**, *132*, 15480-15483.

(8) A. Loudet, K. Burgess, *Chem. Rev*., **2007**, *107*, 4891-4932.

(9) (a) T. Yogo, Y. Urano, Y. Ishitsuka, F. Maniwa, T. Nagano, *J. Am. Chem. Soc*., **2005**, *127*, 12162-12163. (b) N. Adarsh, R.R. Avirah, D. Ramaiah, *Org. Lett*., **2010**, *12*, 5720-5723.

(10) (a) P.D. Frischmann, K. Mahata, F. Würthner, *Chem. Soc. Rev*., **2013**, *42*, 1847-1870. (b) J.Z. Zhao, W.H. Wu, J.F. Sun, S. Guo, *Chem. Soc. Rev*., **2013**, *42*, 5323-5351. (c) A. Kamkaew, S.H. Lim, H.B. Lee, L.V. Kiew, L.Y. Chung, K. Burgess, *Chem. Soc. Rev*., **2013**, *42*, 77-88. (d) L.K.H. Bonardi, F. Camerel, P. Jolinat, P. Retailleau, R. Ziessel, *Adv. Funct. Mater*., **2008**, *18*, 401-413.

(11) J.A. Riddick, W.B. Bunger, T.K. Sakano, Organic Solvents, 4th ed.; Wiley-Interscience, New York, **1986**.

(12) Y.C. Wang, D.K. Zhang, H. Zhou, J.L. Ding, Q. Chen, Y. Xiao, S.X. Qian, *J. Appl. Phys*., **2010**, *108*, 455-462.

(13) K.G. Casey, E.L. Quitevis, *J. Phys. Chem*., **1988**, *92*, 6590-6594.

(14) J.R. Lakowicz, Principles of Fluorescence Spectroscopy, 3rd ed. Analytical and Bioanalytical Chemistry **2008**, *390*, 1223-1224

(15) S. Guo, H.L. Zhang, L. Huang, Z.D. Guo, G. Xiong, J.Z. Zhao, *Chem.Commun*., **2013**, *49*, 8689-8691.

(16) D.C. Wang, J.L. Fan, X.Q. Gao, B.S. Wang, S.G. Sun, X.J. Peng, *J. Org. Chem*., **2009**, *74*, 7675-7683.

(17) A. Vazquez-Romero, N. Kielland, M.J. Arevalo, S. Preciado, R.J. Mellanby, Y. Feng, R. Lavilla, M. Vendre, *J. Am. Chem. Soc*., **2013**, *135*, 16018-16021.

(18) Z.S. Li, Y. Chen, X.J. Lv, W.F. Fu, *New J. Chem*., **2013**, *37*, 3755-3761.

(19) J.H. Gibbs, L.T. Robins, Z.H. Zhou, P. Bobadova-Parvanova, M. Cottam, G.T. McCandless, F.R. Fronczek, M.G.H. Vicente, *Bioorg. Med. Chem*., **2013**, *21*, 5770-5781.

(20) G.N. Schrauzer, *Inorg. Synth*., **1968**, *11*, 61-69.

(21) A. Bakac, M.E. Brynildson, J.H. Espenson, *Inorg. Chem*., **1986**, *25*, 4108-4114.

(22) T. Higashi, ABSCOR, Empirical Absorption Correction based on Fourier series Approximation. Rigaku Corporation: Tokyo, **1995**.

(23) G.M. Sheldrick, SHELXS-97, Program for X-ray Crystal Structure Determination. University of Gottingen: Germany, **1997**.

(24) G.M. Sheldrick, SHELXL-97, Program for X-ray Crystal Structure Refinement. University of Gottingen: Germany, **1997**.

(25) L.J. Barbour, *Supramol. Chem*., **2001**, *1*, 189-191.

(26) A.L. Spek, Implemented as the PLATON Procedure, a Multi-purpose Crystallographic Tool. Utrecht University: Utrecht, the Netherlands, **1998**.

(27) K. Brandenburg, *DIAMON*D, Version 3.1f. Crystal Impact GbR: Bonn, Germany, **2008**.

(28) J. Zhang, Q. Xu, Z. Feng, M. Li, C. Li, *Angew. Chem. Int. Ed*., **2008**, *47*, 1766-1769.

(29) J.H. Yum, P. Chen, M. Grätzel, M.K. Nazeeruddin, *Chemsuschem* **2008**, *1*, 699-707.

(30) M. J. Frisch, G. W. Trucks, H. B. Schlegel, G. E. Scuseria, M. A. Robb, J. R. Cheeseman, G. Scalmani, V. Barone, B. Mennucci, G. A. Petersson, H. Nakatsuji, M. Caricato, X. Li, H. P. Hratchian, A. F. Izmaylov, J. Bloino, G. Zheng, J. L. Sonnenberg, M. Hada, M. Ehara, K. Toyota, R. Fukuda, J. Hasegawa, M. Ishida, T.

Nakajima, Y. Honda, O. Kitao, H. Nakai, T. Vreven, J. A. Montgomery Jr,., J. E. Peralta, F. Ogaliaro, M. Bearpark, J. J. Heyd, E. Brothers, K. N. Kudin, V. N. Staroverov, R. Kobayashi, J. Normand, K. Raghavachari, A. Rendell, J. C. Burant, S. S. Iyengar, J. Tomasi, M. Cossi, N. Rega, J. M. Millam, M. Klene, J. E. Knox, J. B. Cross, V. Bakken, C. Adamo, J. Jaramillo, R. Gomperts, R. E. Stratmann, O. Yazyev, A. J. Austin, R. Cammi, C. Pomelli, J. W. Ochterski, R. L. Martin, K. Morokuma, V. G. Zakrzewski, G. A. Voth, P. Salvador, J. J. Dannenberg, S. Dapprich, A. D. Daniels, O. Farkas, J. B. Foresman, J. V. Ortiz, J. Cioslowski and D. J. Fox, *Gaussian*, Inc., Wallingford CT., **2009**.

(31) A.D. Becke, *J. Chem. Phys*., **1993**, *98*, 5648-5652.

(32) C. Lee, W. Yang, R.G. Parr, *Phys. Rev., B* **1988**, *37*, 785-789.

(33) E. Cances, B. Mennucci, J. Tomasi, *J. Chem. Phys*., **1997**, *107*, 3032-3041.

(34) A.D. Becke, *J. Chem. Phys*., **1993**, *98*, 1372-1377.

(35) A.D. Becke, *J. Chem. Phys*., **1998**, *109*, 2092-2098.

(36) L. Goerigk, S. Grimme, *J. Chem. Phys*., **2010**, *132*, 184103-184109.

(37) (a) Z.H. Pan, G.G. Luo, J.W. Zhou, J.X. Xia, K. Fang, R.B. Wu, *Dalton Trans* **2014**, *43*, 8499-8507. (b) G.G. Luo, K. Fang, J.H. Wu, J.C. Dai, Q.H. Zhao, *Phys. Chem. Chem. Phys*., **2014**, *16*, 23884-23894. (c) Z.H. Pan, J.W. Zhou, G.G. Luo, *Phys. Chem. Chem. Phys*., **2014**, *16*, 16290-16301.

(38) (a) F. D'Souza, P.M. Smith, M.E. Zandler, A.L. McCarty, M. Itou, Y. Araki, O. Ito, *J. Am. Chem. Soc*., **2004**, *126*, 7898-7907. (b) E. Maligaspe, T. Kumpulainen, N.K. Subbaiyan, M.E. Zandler, H. Lemmetyinen, N.V. Tkachenko, F. D'Souza, *Phys. Chem. Chem. Phys*., **2010**, *12*, 7434-7444.

(39) (a) R. Nithya, P. Kolandaivel, K. Senthilkumar, *Mol. Phys*., **2012**, *110*, 445-456. (b) J.B. Prieto, F.L. Arbeloa, V.M. Martinez, T.A. Lopez, I.L. Arbeloa, *Phys. Chem. Chem. Phys*., **2004**, *6*, 4247-4253. (c) D. Jacquemin, S. Chibani, B.L. Guennic, B. Mennucci, *J. Phys. Chem., A* **2014**, *118*, 5343-5348. (d) S. Chibani, A.D. Laurent, B.L. Guennic, D. Jacquemin, *J. Chem. Theory Comput*., **2014**, *10*, 4574−4582.

(40) (a) X.H. Wang, S. Goeb, Z.Q. Ji, N.A. Pogulaichenko, F.N. Castellano, *Inorg. Chem*., **2011**, *50*, 705-707. (b) P.W. Du, J. Schneider, F. Li, W. Zhao, U. Patel, F.N. Castellano, R. Eisenberg, *J. Am. Chem. Soc*., **2008**, *130*, 5056-5058.

(41) J.L. Dempsey, B.S. Brunschwig, J.R. Winkler, H.B. Gray, *Acc. Chem. Res*., **2009**, *42*, 1995-2004.

(42) (a) M. Razavet, V. Artero, M. Fontecave, *Inorg. Chem*., **2005**, *44*, 4786-4795. (b) X. Hu, B.S. Brunschwig, J.C. Peters, *J. Am. Chem. Soc*., **2007**, *129*, 8988-8998.

(43) W.H. Wu, H.M. Guo, W.T. Wu, S.M. Ji, J.Z. Zhao, *J. Org. Chem*., **2011**, *76*, 7056-7064.

(44) J. Bartelmess A.J. Francis, K.A. El Roz, F.N. Castellano, W.W. Weare, R.D. Sommer, *Inorg. Chem*., **2014**, *53*, 4527-4534.

(45) In another photocatalytic hydrogen production systems containing o*rtho*-, *meta*-, and *para*-pyridyl-substitution iodinated BODIPY derivatives as sensitizers, a cobaloxime **C1** as a H_2-evoluting catalyst, *ortho*-pyridyl substituted BODIPY showed the highest efficiency of hydrogen generation. Also, there is a good linear relationship of $\varepsilon \times \Phi_{ISC}$ *versus* TONs of H_2 production for these pyridyl-substituted BODIPYs (see Fig. S11 in the supporting information). The detailed results will be published elsewhere.

(46) D. Rehm, A. Weller, *Ber. Bunsenges. Phys. Chem*., **1969**, *73*, 834-839.

(47) P.W. Du, K. Knowles, R. Eisenberg, A *J. Am. Chem. Soc*., **2008**, *130*, 12576-12577.

(48) L.M. Gong, J. Wang, H. Li, L. Wang, J.H. Zhao, Z.P. Zhu, *Cata. Commun*., **2011**, *12*, 1099-1103.

(49) (a) R. Abe, K. Hara, K. Sayama, K. Domen, H. Arakawa, *J. Photochem. Photobiol., A* **2000**, *137*, 63-69. (b) R. Abe, K. Sayama, H. Arakawa, *J. Photochem. Photobiol., A* **2004**, *166*, 115-122.

(50) A.L. Linsebigler, G. Lu, J.T. Yates, *Chem. Rev*., **1995**, *95*, 735.

(51) A. Patsoura, D.I. Kondarides, X.E. Verykios, *Appl. Catal., B* **2006**, *64*, 171-179.

(52) (a) D. Duonghong, E. Borgarello, M. Gräetzel, *J. Am. Chem. Soc*., **1981**, *103*, 4685-4690. (b) A.J. Bard, *J. Phys. Chem*., **1982**, *86*, 172-177.

(53) (a) G.R. Bamwenda, S. Tsubota, T. Kobayashi, M. Haruta, *J. Photochem. Photobiol., A* **1994**, 77, 59-67. (b) G.R. Bamwenda, S. Tsubota, T. Nakamura, M. Haruta, *J. Photochem. Photobiol., A* **1995**, *89*, 177-189.

(54) (a) R.P. Sabatini, W.T. Eckenhoff, A. Orchard, K.P. Liwosz, M.R. Detty, D.F. Watson, D.W. McCamant, R. Eisenberg, *J. Am. Chem. Soc*. **2014**, *136*, 7740-7750. (b) R. P. Sabatini, T. M. McCormick, T. Lazarides, K. C. Wilson, R. Eisenberg, D. W. McCamant, *J. Phys. Chem. Lett*., 2011, **2**, 223-227. (c) W. Kim, T. Tachikawa, T. Majima, C.H. Li, H.J. Kim, W. Choi, *Energy Environ. Sci*., 2010, **3**, 1789-1795.

(55) A.S. Hart, C.B. KC, H.B. Gobeze, L.R. Sequeira, F. D'Souza, *ACS Appl. Mater., Interfaces* **2013**, *5*, 5314-5323.

(56) (a) M. Pastore, F. De Angelis, *Phys. Chem. Chem. Phys*., **2012**, *14*, 920-928. (b) J.N. Clifford, E. Palomares, M.K. Nazeeruddin, M. Grätzel, J. Nelson, X. Li, N.J. Long, J.R. Durrant, *J. Am. Chem. Soc*., **2004**, *126*, 5225-5233.

(57) S.P. Singh, T. Gayathri, *Eur. J. Org. Chem*., **2014**, 4689-4707.

(58) E. Bae, W. Choi, J. Park, H.S. Shin, S.B. Kim, J.S. Lee, *J. Phys. Chem. B* **2004**, 108, 14093-14101.

(59) (a) R. Huber, S. Spörlein, J.E. Moser, M. Grätzel, J. Wachtveitl, *J. Phys. Chem., B* **2000**, *104*, 8995-9003. (b) S. Kaniyankandy, S. Verma, J.A. Mondal, D.K. Palit, H.N. Ghosh, *J. Phys. Chem., C* **2009**, *113*, 3593-3599. (c) S.G. Bairu, E. Mghanga, J. Hasan, S. Kola, V.J. Rao, K. Bhanuprakash, L. Giribabu, G.P. Wiederrecht, R. Silva, L.G.C. Rego, G. Ramakrishna, *J. Phys. Chem., C* **2013**, *117*, 4824-4835.

(60) M. Pastore, F. De Angelis, *ACS Nano*., **2010**, *4*, 556-562.

Graphical Abstract

BODIPY photosensitizers were used to investigate the relationship of structure and effectiveness of visible-light-driven hydrogen production as well as DSSCs.